

# Micro-displacement sensor based on an asymmetric wavy multimode fiber interferometer\*

LI Yuanzheng, LI Yi\*\*, MIAO Yiping, WANG Fang, HU Kai, and ZHANG Kailiang\*\*

*Tianjin Key Laboratory of Film Electronic and Communication Devices, School of Integrated Circuit Science and Engineering, Engineering Research Center of Optoelectronic Devices & Communication Technology, Ministry of Education, Tianjin University of Technology, Tianjin 300384, China*

(Received 4 August 2022; Revised 26 August 2022)

©Tianjin University of Technology 2023

We proposed a compact and tunable multimode interferometer (MMI) based on an asymmetric wavy fiber (AMWF), which has axial offset, off-center taper waist, and micro-length. The fabrication process only contains non-axis pulling processes of single-mode fiber on two close positions. Theoretical qualitative analyses and experiments verify the tunable multimode propagation of the AMWF. Experimental results show a nonlinear wavelength response with increasing axis displacement from 0 to 120  $\mu\text{m}$ . In the range of 0–10  $\mu\text{m}$ , the sensitivity reaches the highest value of  $-1.33 \text{ nm}/\mu\text{m}$ . Owing to its cost-effective, high-compact and tunable multimode propagation properties, the AMWF provides a promising platform for micro-nano photonic devices and optical sensing applications.

**Document code:** A **Article ID:** 1673-1905(2023)03-0134-5

**DOI** <https://doi.org/10.1007/s11801-023-2139-5>

Since Thomas Young presented double-slit interference experiment in 1807<sup>[1]</sup>, optical interferometer has been one of the major devices for studying the fundamental nature of light and high precision optical metrology in modern science and technology. From monitoring specific interference spectra or patterns, most physical quantities can be decoded<sup>[2]</sup>, such as displacement<sup>[3]</sup>, angle<sup>[4]</sup>, curvature<sup>[5]</sup>, refractive index<sup>[6]</sup>, magnetic field intensity<sup>[7]</sup>, temperature<sup>[8]</sup>, humidity<sup>[9]</sup> and biomolecular behavior<sup>[10]</sup>. Recently, the optical interferometers market continues to grow gradually in higher miniaturization and sensitivity, which play important roles in various industrial and scientific processes, such as astronautics<sup>[11]</sup>, manufacturing<sup>[12]</sup>, structural health monitoring<sup>[13]</sup>, environmental monitoring<sup>[14]</sup>, label-free detection of live cancer cells<sup>[15]</sup>, DNA hybridization<sup>[16]</sup>, and so on.

Compared with conventional optical interferometer, optical fiber interferometers are more highly attractive for future micro-nano optical systems<sup>[17,18]</sup> owing to their obvious advantages, such as light weight, remote signal transmission and electromagnetic immunity. To date, varieties of optical fiber interferometers have been realized by different geometries including Mach-Zehnder interferometer (MZI)<sup>[19]</sup>, Fabry-Perot interferometer<sup>[20]</sup>, and Sagnac interferometer<sup>[21]</sup>. Due to miniaturization, simple fabrication and low cost, the optical fiber MZI is the most appropriate candidate to realize the high per-

formance micro-nano photonic devices, which can be mass-produced.

In addition, for optical fiber MZI, it is quite important to investigate the relationship between structure and physical quantities, for example, the displacement between two ends of the structure<sup>[22]</sup>. Because the light field in optical fiber MZIs can be modulated as the structure stretched, the stretchable optical fiber MZIs can be regarded as tunable interferometers, which is also an effective way for displacement sensing through light field modulation in optical fiber MZIs.

Two-mode interferometer based on single mode fiber (SMF), multimode interferometer (MMI) based on SMF<sup>[23]</sup>, such as bow type optical fiber taper<sup>[24]</sup>, and MMI based on special optical fiber sandwiched between two SMFs<sup>[25]</sup> are main schemes of the optical fiber MZIs for tunable interferometers and displacement sensing. In particular, the MMIs have been widely studied as high-performance optical fiber sensors. However, their precise fabrication process and expensive experimental devices limit their practical applications and large-scale production. Therefore, it is necessary to develop a micro multimode fiber interferometer which not only has high performance, but also has low cost and simple manufacturing process.

In this paper, we present a compact and tunable MMI based on an asymmetric wavy fiber (AMWF), which has

\* This work has been supported by the National Key Research and Development Program of China (No.2017YFB0405600), the National Natural Science Foundation of China (Nos.62001326, 61274113 and 61404091), the Natural Science Foundation of Tianjin City (Nos.18JCYBJC85700 and 18JCZDJC30500), the Open Project of State Key Laboratory of Functional Materials for Information (No.SK202007), and the Science and Technology Planning Project of Tianjin City (No.20ZYQCGX00070).

\*\* E-mails: liyiviolet@outlook.com; kailiang\_zhang2007@163.com

an axial offset and an off-center taper waist. The whole fabrication process only contains non-axis pulling processes on two close fusion positions on a segment of SMF. The AMWF has the advantages of low cost, high integration, high mechanical strength and high-efficiency controlling light propagation, and thus it is practicable to use this AMWF structure-based micro-nano photonic device to allow efficient approach for sensing application.

Fig.1 shows the schematic diagram of our proposed AMWF, which has an axial offset and whose taper waist is off center. A conventional SMF (SMF-28e, Corning, Inc.) we used in this designed structure has the effective indices of 1.468 2/1.462 8 and the core/cladding diameters of 8.2  $\mu\text{m}$ /125  $\mu\text{m}$ . The whole fabrication process of the asymmetric taper waist only contains non-axis pulling processes on two close fusion positions on a segment of SMF, and can be simply realized by the manual mode operation of a commercial fusion splicer (FiTel S178A, Japan). The SMF is firstly fixed by two clamps with an axial offset about 64.2  $\mu\text{m}$  in the fusion splicer. Next, a non-axial pulling ('clean' arc charge and outward shift of 5  $\mu\text{m}$  for the two clamps) is performed and repeated 21 times. Thus, a taper waist is formed at the first discharge position, which is marked in Fig.1. Afterwards, the clamps in the fusion splicer are manually controlled to increase the axial offset to 128.5  $\mu\text{m}$  and move the position of the discharge 64  $\mu\text{m}$ .

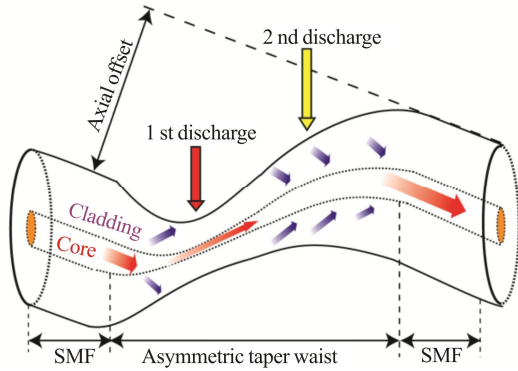


**Fig.1 Schematic diagram of the AMWF**

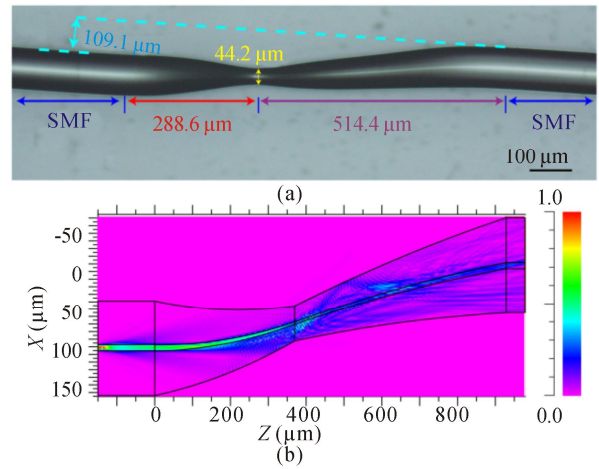
The second discharge position is also marked in Fig.1. Subsequently, a 'clean' arc charge is performed to form an asymmetric structure, which has an axial offset and whose taper waist is off center. The asymmetry can be further enhanced by the clamps outward shift of 5  $\mu\text{m}$ . Finally, when this process repeated 5 times, the AMWF can be fabricated. As shown in Fig.2(a), the axial offset, taper waist and the length of the two asymmetric arms are 109.1  $\mu\text{m}$ , 40.4  $\mu\text{m}$ , 288.6  $\mu\text{m}$  and 514.4  $\mu\text{m}$ , respectively.

Fig.2(b) shows the light propagation in the AMWF utilizing beam propagation method (BPM), as implemented in the Rsoft software. It's clearly seen that a part of light energy is coupled from the fiber core to the cladding in the first bending region, and then coupled back

from the fiber cladding to core in the second bending region, realizing the multiple mode interference, which can be mathematically described by<sup>[26]</sup>

$$I = I_{\text{core}} + \sum_j I_{\text{cladding}}^j + 2 \sum_j \sqrt{I_{\text{core}} I_{\text{cladding}}^j} \cos(\Delta\Phi_j), \quad (1)$$

where  $I_{\text{core}}$  and  $I_{\text{cladding}}^j$  are the light intensities of core mode and the  $j$ -th cladding mode, respectively.  $\Delta\Phi_j$  is the phase difference between core mode and the  $j$ -th cladding mode. Here,  $\Delta\Phi_j = 2\pi\Delta n_{\text{eff}}^j L/\lambda$ , where  $\Delta n_{\text{eff}}^j$  is the effective refractive index difference between the core mode and the  $j$ -th cladding mode, and  $L$  is the length of the effective interference region of the AMWF.



**Fig.2 (a) Microscopic image and (b) simulated light energy distribution of the AMWF**

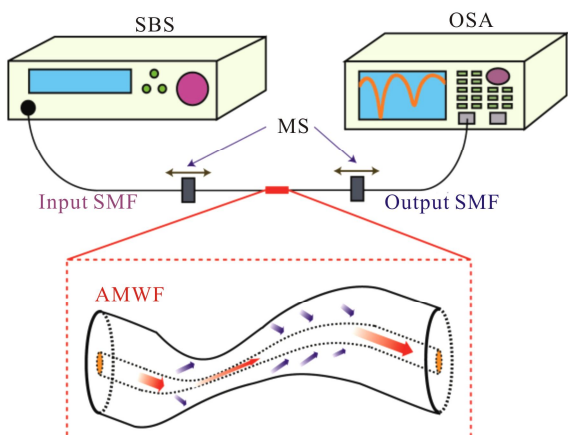
The resonant dip wavelength can be expressed as

$$\lambda_N = \frac{2\Delta n_{\text{eff}}^j L}{2N + 1}, \quad (2)$$

where  $N$  is the interference order in the AMWF.

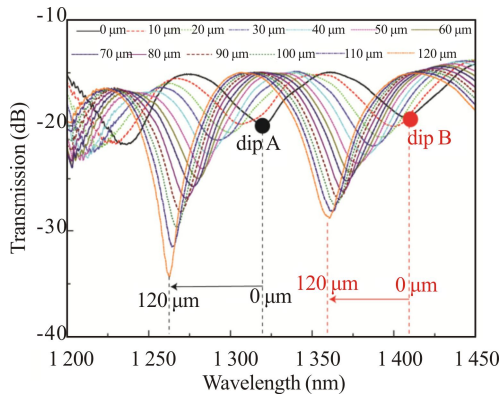
When the displacement between two ends of AMWF changes, the  $\Delta n_{\text{eff}}^j$  and  $L$  can be tuned. According to Eq.(2), the changes in the  $\Delta n_{\text{eff}}^j$  and  $L$  will cause the shifts of the resonant dips of the interference fringes. Thus, by tuning the axial displacement of the AMWF, the propagation characteristics of the AMWF can be modulated. Moreover, the axial displacement sensing can be achieved by monitoring the shifts of the interference fringes.

The experimental setup for the axial micro-displacement tunability is shown in Fig.3, which consists of a supercontinuum broadband source (SBS, wavelength ranges from 600 nm to 1 700 nm), an optical spectrum analyzer (OSA: Yokogawa AQ6370C), and two micro-motion stages (MSs). The two clamps on the MSs are fixed on the two ends of the AMWF respectively, and are manually controlled until the AMWF is straight. In this situation, the position of the right clamp is regarded as the initial axial micro-displacement ( $\Delta L=0$   $\mu\text{m}$ ) in our experiment. By moving the right clamp with a step interval of 10  $\mu\text{m}$ , we can monitor the shift of the transmission dip wavelength with the increasing axial micro-displacement.



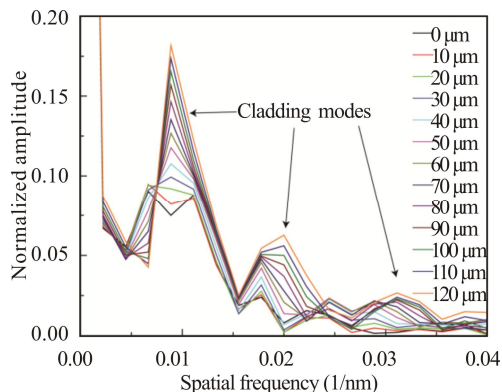
**Fig.3 Experimental setup for the axial micro-displacement measurement**

Fig.4 shows the transmission spectra of the AMWF under different axial micro-displacements with an increment of 10  $\mu\text{m}$  from 0 to 120  $\mu\text{m}$ . It can be observed that as the axial displacement between two ends of the AMWF increases, the resonant dips A and B move to a shorter wavelength. In fact, the axial displacement increasing can lead to the elongation of the AMWF and the change of the  $n_{\text{eff}}$  of the fiber core and cladding modes. According to Eq.(2), clearly, the influence of the decrease in the  $\Delta n_{\text{eff}}$  has a stronger impact than the increase of the effective interference region of the AMWF, as the axial displacement increasing in our experiment.



**Fig.4 Transmission spectra of the AMWF under different axial micro-displacements at a variation step of 10  $\mu\text{m}$**

In order to understand the transmission characteristics of the AMWF, the fast Fourier transform (FFT) method is used to obtain the spatial frequency spectra of the transmission spectra shown in Fig.4. The corresponding results are depicted in Fig.5. It is clearly seen that there are several cladding modes involved in the transmission spectra, which demonstrates that the AMWF is an MMI. Moreover, as the axial displacement increases, the positions of the cladding modes can be modulated and the amplitudes increase.



**Fig.5 Spatial frequency spectra of the transmission spectra shown in Fig.4**

The relationships between the axial displacement and the wavelength of the resonant dips are shown in Fig.6. The shifts of the dips A and B are fitted by an exponential function with a high coefficient  $R^2$  of 0.997 84 and 0.997 81, respectively. The sensitivities decrease with the axial micro-displacement increasing. For dip A, the axial micro-displacement sensitivity can reach the highest value of  $-1.33 \text{ nm}/\mu\text{m}$  in the range of 0—10  $\mu\text{m}$ . In the range of 50—120  $\mu\text{m}$ , the wavelength shift of dip A can approximately be seen as a linear relationship against the increase of the axial micro-displacement, with the sensitivity of  $-0.303 \text{ nm}/\mu\text{m}$ . For dip B, in the ranges of 0—20  $\mu\text{m}$  and 60—120  $\mu\text{m}$ , the sensitivities are estimated to be  $-0.736 \text{ nm}/\mu\text{m}$  and  $-0.23 \text{ nm}/\mu\text{m}$ , respectively.

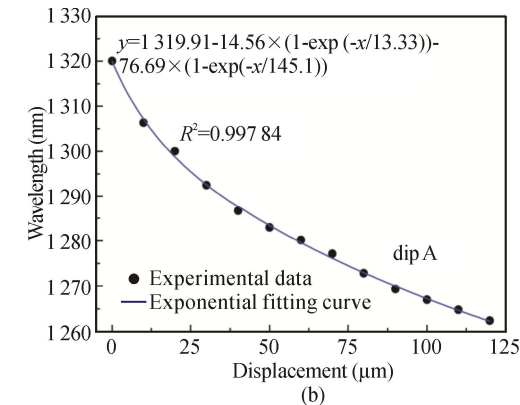
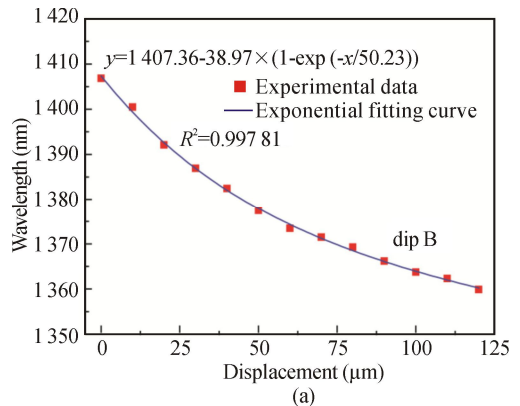


**Fig.6 Wavelengths of (a) dip B and (b) dip A as a function of the axial micro-displacement**

A comparison of performances between the proposed AMWF and other micro-MZIs is summarized in Tab.1. Compared with other micro-MZIs, our proposed AMWF reveals a relatively high sensitivity and a micro-length. Besides, the proposed AMWF sensor is fabricated only using fused tapering process based on SMF, the diameter of the tapered waist is only 44.2  $\mu\text{m}$ , and the length is shorter than 1 mm, which make this sensor have rapid and simple fabrication process, low cost, more mechanical stability, and sensing in micro restrained space.

**Tab.1 Sensor performances of the proposed AMWF in comparison with other papers**

Micro-MZI RI sensors	Sensitivity	Displacement range ( $\mu\text{m}$ )	Sensor length (mm)	Reference
Two S-bend fibers	-1.533 nm/ $\mu\text{m}$ and -0.833 nm/ $\mu\text{m}$	0—200	2.3	[22]
A bowknot- type taper	-0.385 dB/ $\mu\text{m}$	0—62	18	[24]
Thin-core fiber modal interfer- ometer	-0.015 35 nm/ $\mu\text{m}$	0—600	27	[27]
The pro- posed AMWF	-1.33 nm/ $\mu\text{m}$ and -0.303 nm/ $\mu\text{m}$	0—120	0.803	

In conclusion, we propose and demonstrate a compact and tunable MMI based on an AMWF, which has an axial offset and an off-center taper waist. The AMWF has a compact length of 803  $\mu\text{m}$ , ensuring good mechanical strength, and can realize sensing in limited space. The AMWF is only fabricated by two non-axis pulling processes on a segment of SMF. The multimode propagation characteristics of the proposed AMWF are also theoretically and experimentally demonstrated. In addition, the propagation characteristics can be modulated by tuning the axial displacement of the AMWF. The experiment results show that there is a nonlinear wavelength response with increasing displacement from 0 to 120  $\mu\text{m}$ . The sensitivities decrease with the axial micro-displacement increasing. In the displacement range of 0—10  $\mu\text{m}$ , the sensitivity can reach the highest value of -1.33 nm/ $\mu\text{m}$ . Our proposed AMWF has the advantages of high cost-efficiency, high integration, high mechanical strength and high-efficiency controlling light propagation, thus it would be of great significance for developing new micro-nano photonic devices and an efficient platform for optical sensing applications.

### Acknowledgements

The authors would like to extend their appreciation to Tianjin Yiyang Technology Co., Ltd. for support to this work.

### Statements and Declarations

The authors declare that there are no conflicts of interest related to this article.

### References

- [1] YOUNG T. A course of lectures on natural philosophy and the mechanical arts V2[M]. New York: Manhattan Rare Book Company, 1807.
- [2] SMITH T A, SHIH Y. Turbulence-free double-slit interferometer[J]. Physical review letters, 2018, 120(6): 063606.
- [3] LIU T, PAGLIANO F, VELDHOVEN R V, et al. Integrated nano-optomechanical displacement sensor with ultrawide optical bandwidth[J]. Nature communications, 2020, 11(1): 1-7.
- [4] HUANG L, XUE J, GAO B, et al. One-dimensional angular-measurement-based stitching interferometry[J]. Optics express, 2018, 26(8): 9882-9892.
- [5] MARRUJO-GARCÍA S, HERNÁNDEZ-ROMANO I, TORRES-CISNEROS M, et al. Temperature-independent curvature sensor based on in-fiber Mach-Zehnder interferometer using hollow-core fiber[J]. Journal of lightwave technology, 2020, 38(15): 4166-4173.
- [6] FLORES-BRAVO J A, ILLARRAMENDI M A, ZUBIA J, et al. Optical fiber interferometer for temperature-independent refractive index measuring over a broad range[J]. Optics & laser technology, 2021, 139: 106977.
- [7] JIANG C, LIU Y, MOU C, et al. Fiber vector magnetometer based on polarization-maintaining fiber long-period grating with ferrofluid nanoparticles[J]. Journal of lightwave technology, 2022, 40(8): 2494-2502.
- [8] DU D, XU C, YANG Z, et al. Ultrasensitive temperature sensor and mode converter based on a modal interferometer in a two-mode fiber[J]. Optics express, 2021, 29(20): 32135-32148.
- [9] HU Z, CHEN Y, TAN J, et al. A hybrid self-growing polymer microtip for ultracompact and fast fiber humidity sensing[J]. Sensors and actuators B: chemical, 2021, 346: 130462.
- [10] LI L, ZHANG Y, ZHOU Y, et al. Optical fiber optofluidic bio-chemical sensors: a review[J]. Laser & photonics reviews, 2021, 15(7): 2000526.
- [11] XIA F, ZHAO Y, HU H, et al. Optical fiber sensing technology based on Mach-Zehnder interferometer and orbital angular momentum beam[J]. Applied physics letters, 2018, 112(22): 221105.
- [12] CUI J, LIU Z, GUNAWARDENA D S, et al. Two-dimensional vector accelerometer based on Bragg gratings inscribed in a multi-core fiber[J]. Optics express, 2019, 27(15): 20848-20856.
- [13] AZMI A I, ABDULLAH A S, NOOR M Y M, et al. Dynamic bending and rotation sensing based on high coherence interferometry in multicore fiber[J]. Optics &

- laser technology, 2021, 135: 106716.2
- [14] ZHONG Y, XU P, YANG J, et al. Optical fiber interferometric humidity sensor by using hollow core fiber interacting with gelatin film[J]. *Sensors*, 2022, 22(12): 4514.
- [15] FARASAT M, AALAEI E, KHEIRATI RONIZI S, et al. Signal-based methods in dielectrophoresis for cell and particle separation[J]. *Biosensors*, 2022, 12(7): 510.
- [16] GONG P, WANG Y, ZHOU X, et al. In situ temperature-compensated DNA hybridization detection using a dual-channel optical fiber sensor[J]. *Analytical chemistry*, 2021, 93(30): 10561-10567.
- [17] ZHU C, HUANG J. Sensitivity-enhanced microwave-photonic optical fiber interferometry based on the Vernier effect[J]. *Optics express*, 2021, 29(11): 16820-16832.
- [18] WEI F, LIU D, WANG Z, et al. Enhancing the visibility of Vernier effect in a tri-microfiber coupler fiber loop interferometer for ultrasensitive refractive index and temperature sensing[J]. *Journal of lightwave technology*, 2020, 39(5): 1523-1529.
- [19] YUAN W, ZHAO Q, LI L, et al. Simultaneous measurement of temperature and curvature using ring-core fiber-based Mach-Zehnder interferometer[J]. *Optics express*, 2021, 29(12): 17915-17925.
- [20] ALONSO-MURIAS M, MONZÓN-HERNÁNDEZ D, ANTONIO-LOPEZ E, et al. Hybrid optical fiber Fabry-Perot interferometer for nano-displacement sensing[J]. *Optics & laser technology*, 2022, 155: 108426.
- [21] FILOTEO-RAZO J D, HERNANDEZ-GARCIA J C, ESTUDILLO-AYALA J M, et al. Multi-wavelength Er-Yb-doped fibre ring laser using a double-pass Mach-Zehnder interferometer with a Sagnac interferometer[J]. *Optics & laser technology*, 2021, 139: 106994.
- [22] CHEN J, ZHOU J, YUAN X. M-Z interferometer constructed by two S-bend fibers for displacement and force measurements[J]. *IEEE photonics technology letters*, 2014, 26(8): 837-840.
- [23] YANG R, YU Y S, CHEN C, et al. S-tapered fiber sensors for highly sensitive measurement of refractive index and axial strain[J]. *Journal of lightwave technology*, 2012, 30(19): 3126-3132.
- [24] SHEN C, WANG Y, CHU J, et al. Optical fiber axial micro-displacement sensor based on Mach-Zehnder interferometer[J]. *Optics express*, 2014, 22(26): 31984-31992.
- [25] LI C, NING T, ZHANG C, et al. All-fiber multipath Mach-Zehnder interferometer based on a four-core fiber for sensing applications[J]. *Sensors and actuators A: physical*, 2016, 248: 148-154.
- [26] ZHANG C, LU P, LIAO H, et al. Simultaneous measurement of axial strain and temperature based on a Z-shape fiber structure[J]. *IEEE photonics journal*, 2017, 9(4): 1-8.
- [27] WU J, MIAO Y, SONG B, et al. Simultaneous measurement of displacement and temperature based on thin-core fiber modal interferometer[J]. *Optics communications*, 2015, 340: 136-140.